Performance Improvement Using Interpulse Pattern Diversity with Space-Time Adaptive Processing

Phillip M. Corbell, M.S.E.E., Air Force Institute of Technology
Michael A. Temple, Ph.D., Air Force Institute of Technology
Todd B. Hale, Ph.D., Air Force Institute of Technology
William P. Baker, Ph.D., Air Force Institute of Technology
Muralidhar Rangaswamy, Ph.D., Air Force Research laboratory/SNHE

Key Words: Transmit Pattern Diversity, AESA, STAP

SUMMARY & CONCLUSIONS

This work investigates the impact of interpulse (pulse-to-pulse) transmit pattern diversity on Space-Time Adaptive Processing (STAP) performance. It is shown that varying interpulse transmit characteristics within a Coherent Processing Interval (CPI) can re-shape the clutter power spectrum, resulting in a interference whitening effect. For conducting comparative analysis with non-adaptive transmit techniques, a commonly used clutter model is extended to effectively incorporate interpulse pattern diversity effects. The work shows promise for achieving better Minimum Discernable Velocity (MDV) using phased array transmit weights derived from optimum STAP weights (known covariance). Pattern diversity effectively re-distributes clutter energy away from the clutter ridge. For the unambiguous clutter case, the proposed adaptive transmit technique shows promise for improving MDV at the clutter ridge peak.

1. INTRODUCTION

A rich and diverse collection of adaptive signal processing algorithms and techniques exist to process received radar data while focusing on system performance optimization under specific criteria. However, relatively few adaptive techniques have been proposed that optimize the energy *transmitted* in pursuit of improving system performance. Systems that adapt to the environment on transmit may unlock previously unreachable levels of performance by exploiting "priors" in a Baysian framework. In pursuing the power of a-priori information, emphasis has been recently placed on designing knowledge-aided adaptive radars [1] and developing adaptive transmit architectures [2]. Such efforts have explored the impact of pulse shaping [3], polarization matching [4], frequency hopping, and other waveform coding/modulation schemes on system performance measures, including target detection [3] and identification [5, 6] both without and with clutter present [7].

With the aid of modern Active Electronically Scanned Array (AESA) technology, techniques involving rapid radar mode switching, transmit beam shaping, pattern dithering, and multiple beam search modes are becoming common place. Such capabilities are made possible through the creation of very agile and flexible antenna patterns. Stimson [8] indicates that to stabilize the transmit beam in response to aircraft dynamics, an AESA must be able to update patterns at rates up to 2 kHz. Thus, it appears the technology exists to switch transmit antenna patterns on an interpulse (pulse-to-pulse) basis, at least for low Pulse Repetition Frequencies (PRFs). Presuming this capability exists, it is reasonable to investigate if some measure of system performance can be enhanced by adaptively changing transmit pattern characteristics on an interpulse basis.

The environmental adaptivity afforded by STAP weighting has been shown to provide large performance gains in receiver processing by jointly working across temporal and spatial domains. Viewing phased array antenna weights as digital filters applied to sampled radar returns, it is reasonable to consider what might be achieved through interpulse application of diverse complex antenna weights applied during pulse *transmission*. Such an application of changing antenna weights creates a different antenna pattern on each pulse, through which the temporal and spatial characteristics of the clutter returns may be affected through *transmit* pattern diversity. Additionally, these antenna weights could be generated adaptively using a-priori channel information, e.g. clutter characteristics estimated during the previous Coherent Processing Interval (CPI), to generate transmit antenna weights for the current CPI pulse train.

This work investigates the impact of implementing interpulse transmit pattern diversity, a technique which brings to bear space-time adaptivity through the antenna pattern on transmit. First, the clutter model of [9, 10] is expanded to incorporate the effects of using different antenna transmit patterns on an interpulse basis. Next, a process for extracting complex transmit weights from the optimum Wiener (receive) filter weights is introduced. Output SINR results are provided using the Wiener filter derived transmit weights to achieve interpulse pattern diversity. Fully-adaptive Matched Filter (MF) and non-adaptive Signal Match (SM) [11] processor results are presented for comparison. Using identical simulation parameters, results achieved with transmit pattern diversity are compared to those where no transmit diversity is employed. Results show that interpulse transmit pattern diversity can alter the structure of the space-time clutter power spectrum. Clutter power density analysis is presented to qualitatively explain noted impacts.

2. EXTENDED CLUTTER MODEL

This work uses clutter models originally developed in [9] and [10]. To simplify the analysis, range ambiguous clutter returns, internal clutter motion, and other decorrelating effects were not included in the results. Simulation parameters are

Report Documentation Page

Form Approved
OMB No. 0704-0188

1. REPORT DATE	2. REPORT TYPE	3. DATES COVERED
01 MAY 2005	**N/A**	**-**

4. TITLE AND SUBTITLE	5a. CONTRACT NUMBER
Performance Improvement Using Interpulse Pattern Diversity with Space-Time Adaptive Processing	5b. GRANT NUMBER
	5c. PROGRAM ELEMENT NUMBER
6. AUTHOR(S)	5d. PROJECT NUMBER
	5e. TASK NUMBER
	5f. WORK UNIT NUMBER
7. PERFORMING ORGANIZATION NAME(S) AND ADDRESS(ES) **Air Force Institute of Technology**	8. PERFORMING ORGANIZATION REPORT NUMBER
9. SPONSORING/MONITORING AGENCY NAME(S) AND ADDRESS(ES)	10. SPONSOR/MONITOR'S ACRONYM(S)
	11. SPONSOR/MONITOR'S REPORT NUMBER(S)

12. DISTRIBUTION/AVAILABILITY STATEMENT
Approved for public release, distribution unlimited

13. SUPPLEMENTARY NOTES
See also ADM002017. Proceedings of the 2005 IEEE International Radar Conference Record Held in Arlington, Virginia on May 9-12, 2005. U.S. Government or Federal Purpose Rights License., The original document contains color images.

14. ABSTRACT

15. SUBJECT TERMS

16. SECURITY CLASSIFICATION OF:			17. LIMITATION OF ABSTRACT	18. NUMBER OF PAGES	19a. NAME OF RESPONSIBLE PERSON
a. REPORT	b. ABSTRACT	c. THIS PAGE			
unclassified	**unclassified**	**unclassified**	**UU**	**6**	

Table 1: Clutter simulation parameters.

Variable	Value
M (pulses in CPI)	8
N (number of azimuth elements)	16
ϕ (Azimuth Transmit Direction)	0^o
θ (Elevation Transmit Direction)	0^o
f_o (carrier frequency)	1240 MHz
f_r (pulse repetition frequency)	1984 Hz
τ (pulse width)	0.8 μs
P_t (transmit power)	200 kW
B (bandwidth)	800 kHz
F_n (receiver noise figure)	3 dB
N_c (number of clutter patches)	360
h_a (aircraft altitude)	3073 m
β (clutter ridge slope)	1
R (target range)	66 km
γ (clutter gamma)	-3 dB
Array Transmit Gain	22 dB (fixed)
Element Pattern	Cosine
Element Gain	4 dB
Element Backlobe Level	-30 dB
d_x (inter-element spacing, x-axis)	$c/\left(2f_0\right)$ m
Transmit Taper	Uniform (None)
L_s (system losses)	3 dB

shown in Table 1 and are partly based on those used by the Multi-Channel Airborne Radar Measurement (MCARM) program. Notation in the following development is consistent with that of [10], i.e., scalars are lowercase, vectors are lowercase and bold, and matrices are uppercase and bold.

Extending the original clutter model to incorporate interpulse pattern diversity effects required modification of the complex received clutter patch voltage α_{ik} and the Doppler steering vector $\mathbf{b}(\bar{\omega}_{ik})$, as contained in the *clutter space-time snapshot* $\boldsymbol{\chi}_c$ given by [9, 10],

$$\boldsymbol{\chi}_c = \sum_{i=0}^{N_r-1} \sum_{k=0}^{N_c-1} \alpha_{ik} \mathbf{b}(\bar{\omega}_{ik}) \otimes \mathbf{a}(\vartheta_{ik}) \tag{1}$$

where N_r indicates the total number of range rings ($N_r = 1$ for the results presented herein), N_c indicates the number of clutter "patches" which segment that ring, $\mathbf{b}(\bar{\omega}_{ik})$ is the temporal (Doppler) steering vector, $\otimes$ is the Kronecker product, and $\mathbf{a}(\vartheta_{ik})$ is a spatial (azimuth) steering vector [10]. In the clutter snapshot of (1), the α_{ik} term represents the complex received voltage of a single clutter patch return which can be represented by [10]

$$\alpha_{ik} = a_{ik} e^{j\psi_{ik}} \tag{2}$$

where ψ_{ik} is the random phase and a_{ik} is the random amplitude of M received pulses from the (i^{th}, k^{th}) clutter patch. Received voltage α_{ik} is randomized in magnitude and phase to account for variability of clutter returns on a patch-to-patch basis. Assuming adjacent clutter patch responses are statistically independent [10], the power statistics of α_{ik} are characterized by

$$\mathcal{E}\{\alpha_{ik}\alpha_{ln}^*\} = \sigma^2 \xi_{ik} \delta_{i-l} \delta_{k-n} \tag{3}$$

where $\sigma^2 = N_0 B$ is the noise power and ξ_{ik} is the per element, per pulse clutter-to-noise power ratio (CNR) defined as [10]

$$\xi_{ik} = \frac{P_t G(\theta_i, \phi_k) g(\theta_i, \phi_k) \lambda_0^2 \sigma_{ik}}{(4\pi)^3 N_0 B L_s R_i^4} \tag{4}$$

In (4), P_t is the transmit power, $G(\theta_i, \phi_k)$ is the transmit antenna power pattern, $g(\theta_i, \phi_k)$ is the receive element power pattern, λ_0 is the wavelength, σ_{ik} is the RCS of the k^{th} clutter patch on the i^{th} range ring, N_0 is the noise Power Spectral Density (PSD), B is the system bandwidth, L_s is the system losses, and R_i is the range to the i^{th} range ring. Traditionally, the per pulse CNR given by (4) is constant across all M pulses. However, when implementing interpulse pattern diversity, the transmit antenna power pattern $G(\theta_i, \phi_k)$ varies from pulse-to-pulse. To properly vectorize the time varying effects, it is useful to separate the pulse dependent transmit array factor from (4) and define the remaining (pulse independent) expression as $\tilde{\xi}_{ik}$:

$$\xi_{ikm} = \left|W_m(\theta_i, \phi_k)\right|^2 \tilde{\xi}_{ik} \tag{5}$$

$$\tilde{\xi}_{ik} = \frac{P_t g^2(\theta_i, \phi_k) \lambda_0^2 \sigma_{ik}}{(4\pi)^3 N_0 B L_s R_i^4} \tag{6}$$

where ξ_{ikm} and $W_m(\theta_i, \phi_k)$ are the CNR and complex voltage transmit array factor, respectively, for the m^{th} pulse in the CPI. Equivalence of (4) and (5) can be shown using (6) and the relationship between the transmit antenna power pattern, array factor, and antenna element power patterns given by:

$$G(\theta_i, \phi_k) = |W_m(\theta_i, \phi_k)|^2 g(\theta_i, \phi_k) \tag{7}$$

In addition to the array factor magnitude $|W_m(\theta_i, \phi_k)|$, the transmit array factor phase $\measuredangle\left[W(\theta_i, \phi_k)\right]$ must also be considered. Typically, the transmit array pattern remains constant over the CPI and the array's phase response is accounted for in the random phase term ψ_{ik} of (2). However, when transmit pattern diversity is employed, the array's phase response is a function of the m^{th} pulse, i.e. $\measuredangle\left[W_m(\theta_i, \phi_k)\right]$, preventing its absorbtion into ψ_{ik} of (2). Thus, the modified received voltage expression for the m^{th} pulse is obtained by expanding (2) as follows:

$$\alpha_{ikm} = a_{ikm} e^{j\measuredangle[W_m(\theta_i, \phi_k)]} e^{j\psi_{ik}} \tag{8}$$

Given the pulse dependence of ξ_{ikm} in (5), the equivalence of (5) to (4), and the relationship given by (3), it is clear that the received voltage magnitude a_{ikm} in (8) is pulse dependent. To properly vectorize the transmit interpulse pattern diversity effects it is necessary to expand a_{ikm} into pulse independent and pulse dependent factors. This is done by defining a_{ikm} as

$$a_{ikm} = \tilde{a}_{ik} |W_m(\theta_i, \phi_k)| \tag{9}$$

where $\tilde{a}_{ik}$ is the pulse independent received amplitude response which is constant across the CPI of M pulses but random across clutter patches. Substituting (9) into (8), the received clutter voltage for the m^{th} pulse becomes

$$\begin{aligned} \alpha_{ikm} &= \tilde{a}_{ik} \left\{ |W_m(\theta_i, \phi_k)| e^{j\measuredangle[W_m(\theta_i, \phi_k)]} \right\} e^{j\psi_{ik}} \\ &= \tilde{a}_{ik} e^{j\psi_{ik}} W_m(\theta_i, \phi_k) \end{aligned} \tag{10}$$

which, on a per pulse basis, can be shown to have the same power statistics as the original clutter voltage (2), i.e.

$$\mathcal{E}\{\alpha_{ikm}\alpha_{lnm}^*\} = \sigma^2 \xi_{ikm} \delta_{i-l} \delta_{k-n} \tag{11}$$

Furthermore, the pulse independent portions of the received voltage and the CNR equations are related by

$$\mathcal{E}\{\tilde{a}_{ik}\tilde{a}_{ln}\} = \sigma^2\tilde{\xi}_{ik}\delta_{i-l}\delta_{k-n} \tag{12}$$

It can be shown that substituting α_{ikm} of (10) for α_{ik} in (1), while using the definition of $\tilde{\xi}_{ik}$ in (6), results in an equivalent space time snapshot given by (1) when the transmit array factor $W_m(\theta_i, \phi_k)$ is identical for all M pulses in the CPI. To incorporate a time-varying transmit array factor into the development, the pulse dependent portion of (10) must be vectorized temporally.

To vectorize the transmit array factor, let $\mathbf{W}(\theta_i, \phi_k)$ be a $M \times 1$ complex vector containing the complex transmit array factor for each pulse in the CPI, i.e.,

$$\mathbf{W}(\theta_i, \phi_k) = \begin{bmatrix} W_1(\theta_i, \phi_k) \\ W_2(\theta_i, \phi_k) \\ \vdots \\ W_M(\theta_i, \phi_k) \end{bmatrix}. \tag{13}$$

As provided in linear array pattern theory [12], phased array weights determine the spatial array factor through an inner product. For a given pulse m and transmit direction (θ_i, ϕ_k), the complex array factor can be expressed as

$$W_m(\theta_i, \phi_k) = \mathbf{w}_{\mathrm{TX}m}^H \mathbf{a}(\theta_i, \phi_k) \tag{14}$$

where $\mathbf{w}_{\mathrm{TX}m}$ represents a $N \times 1$ phased array transmit weight vector for the m^{th} pulse and $\mathbf{a}(\theta_i, \phi_k)$ is a spatial steering vector pointing at the i^{th} clutter patch, and the k^{th} range ring. Using (14), (13) can also be written as

$$\mathbf{W}(\theta_i, \phi_k) = \begin{bmatrix} \mathbf{w}_{\mathrm{TX1}}^H \mathbf{a}(\theta_i, \phi_k) \\ \mathbf{w}_{\mathrm{TX2}}^H \mathbf{a}(\theta_i, \phi_k) \\ \vdots \\ \mathbf{w}_{\mathrm{TXM}}^H \mathbf{a}(\theta_i, \phi_k) \end{bmatrix}. \tag{15}$$

Having vectorized the array factor temporally, it must also be vectorized spatially to be dimensionally compatible with (1). Since transmit pattern effects are identical across the antenna element returns for a given transmit direction of (θ_i, ϕ_k), the set of M complex antenna patterns can be cast into the space-time steering vector format $(1 \times NM)$ using the Kronecker product $\otimes$ as follows:

$$\mathbf{W}(\theta_i, \phi_k) \otimes \mathbf{1}_N \tag{16}$$

where $\mathbf{1}_N$ represents a $N \times 1$ vector of ones. Using (13) and (16), (10) can be vectorized as

$$\begin{aligned} \boldsymbol{\alpha}_{ik} &= \tilde{a}_{ik} e^{j\psi_{ik}} \mathbf{W}(\theta_i, \phi_k) \otimes \mathbf{1}_N \\ &= \tilde{\alpha}_{ik} \mathbf{W}(\theta_i, \phi_k) \otimes \mathbf{1}_N \end{aligned} \tag{17}$$

Replacing α_{ik} in (1) with (17), the modified *clutter space-time snapshot* can be written as:

$$\boldsymbol{\chi}_c = \sum_{i=0}^{N_r-1} \sum_{k=0}^{N_c-1} \tilde{\alpha}_{ik} \tilde{\mathbf{b}}(\theta_i, \phi_k, \bar{\omega}_{ik}) \otimes \mathbf{a}(\vartheta_{ik}) \tag{18}$$

The modified Doppler steering vector in (18) is defined as

$$\tilde{\mathbf{b}}(\theta_i, \phi_k, \bar{\omega}_{ik}) = \mathbf{W}(\theta_i, \phi_k) \odot \mathbf{b}(\bar{\omega}_{ik}) \tag{19}$$

where $\odot$ represents the Hadamard (element-wise) product. Using (18), the modified clutter covariance matrix can be computed and written as

$$\mathbf{R}_c = \mathcal{E}\{\boldsymbol{\chi}_c \boldsymbol{\chi}_c^H\} \tag{20}$$

$$\mathbf{R}_c = \sigma^2 \sum_{i=0}^{N_r-1} \sum_{k=0}^{N_c-1} \tilde{\xi}_{ik} (\tilde{\mathbf{b}}_{ik} \tilde{\mathbf{b}}_{ik}^H) \otimes (\mathbf{a}_{ik} \mathbf{a}_{ik}^H) \tag{21}$$

Structurally, the basic form of the modified clutter model remains unchanged from [9, 10] through modification of the clutter-to-noise ratio $\tilde{\xi}_{ik}$, received voltage $\tilde{\alpha}_{ik}$, and the Doppler steering vector $\tilde{\mathbf{b}}_{ik}$ terms. It can be shown that when transmit pattern diversity is not employed, i.e., $W_m(\theta_i, \phi_k)$ is identical for all M pulses in the CPI, the extended clutter model presented herein is equivalent to the original model of [9, 10].

The redefinition of Doppler steering vector $\tilde{\mathbf{b}}(\theta_i, \phi_k, \bar{\omega}_{ik})$ given by (19) provides significant insight into the benefits of transmit pattern diversity. Whereas in the original radar model the clutter patch's temporal Doppler response $\mathbf{b}(\bar{\omega}_t)$ was only a function of normalized target Doppler $\bar{\omega}_{ik}$, the addition of transmit interpulse pattern diversity has induced an additional dependence on the ordered set of transmit patterns represented by $\mathbf{W}(\theta_i, \phi_k)$ of (13). Thus, for a given clutter patch "location" (θ_i, ϕ_k), the patch's Doppler response can be *controlled* by modifying the transmit antenna weights (13) on an interpulse basis. Furthermore, the next section reveals that this capability allows the radar to *affect* the clutter spectral characteristics through *transmit pattern diversity*.

3. TRANSMIT PATTERN DIVERSITY

Given the required AESA flexibility and the ability to model M distinct transmit antenna patterns in the radar data model, focus switches to the issue of generating interpulse transmit patterns. This process is anticipated to be as varied and critical to overall performance as the weight estimation process is for STAP receive processing. One relatively simple implementation first explored here involves using the ideal STAP weights to generate the transmit patterns. To investigate the feasibility of this approach, the procedure detailed below and graphically depicted in Fig. 1 was established.

First, a standard transmit pattern is used to generate known clutter covariance matrix $\mathbf{R_c}$ as detailed along the left-hand side of Fig. 1. This process is referred to herein as *Standard TX*, or *STX* for short. The "TX Antenna Model" block calculates the transmit array factor $W(\theta_i, \phi_k)$ for any normalized $(\mathbf{w}^H\mathbf{w} = N)$ set of antenna weights. The standard transmit power pattern for a given direction (0^o azimuth, 0^o elevation) and corresponding phase response for a linear 16 element array is shown in Fig. 2. The clutter model is then used to generate a known, (ideal) clutter covariance matrix $\mathbf{R_c}$ which is added to noise covariance matrix $\mathbf{R_n}$ to form the ideal clutter-plus-noise covariance matrix $\mathbf{R}$.

As depicted along the right-hand-side of Fig. 1, the *Adaptive TX* process, or *ATX*, generates complex element weights from the covariance matrix $\mathbf{R}$ using the well-known optimum (maximum SINR) fully-adaptive weight set given by

$$\mathbf{w} = \mathbf{R}^{-1}\mathbf{v} \tag{22}$$

where $\mathbf{v}$ is the space-time steering vector representing a target

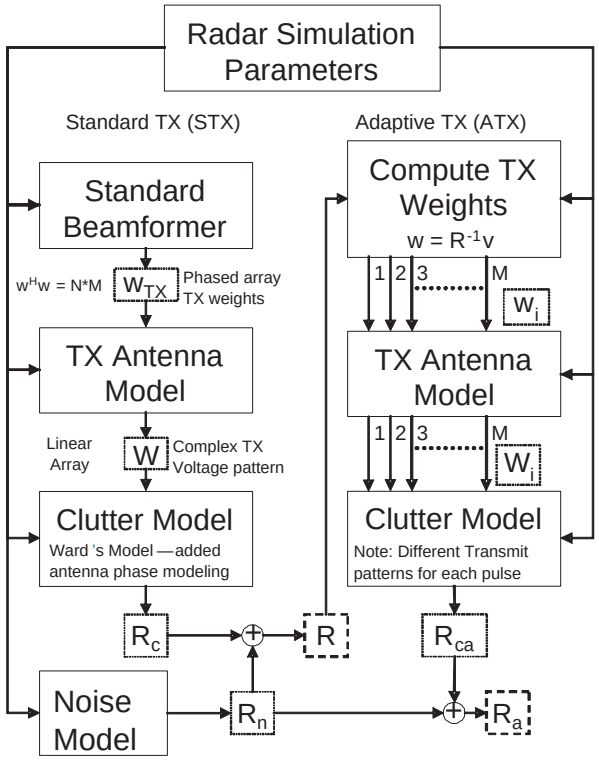

Figure 1: Processing Flow for Standard Transmit (STX) Model and Adaptive Transmit (ATX) Model Using Common Radar Simulation Parameters

response, defined as

$$\mathbf{v} = \mathbf{b}(\bar{\omega}_t) \otimes \mathbf{a}(\theta_t, \phi_t) \tag{23}$$

Using this approach, the ATX method is inherently optimized to search for a given target Doppler frequency and location. One of the more critical areas for any airborne radar is the performance near the main beam clutter, thus this technique is examined by steering the space-time steering vector $\mathbf{v}$ of (23) to a position near the clutter ridge. The results presented here are derived using ATX weights generated for a transmit direction of 0^o in both azimuth and elevation and a "transmit Doppler" value of 0.001 Hz, a position just slightly offset from the peak of the main lobe clutter spectrum response. The use of a "transmit" 0.001 Hz Doppler value in generating ATX patterns was found to give drastically different patterns than when using a 0 Hz Doppler offset.

Given the construction of $\mathbf{v}$ via the Kronecker product, the $MN \times 1$ dimensional weight vector $\mathbf{w}$ can be parsed into M sets of $N \times 1$ spatial weight vectors and used as transmit array weights for each pulse transmitted in the "next" CPI of M pulses. The simulated results presented here are for $M = 8$ pulses and are representative of results obtained for other values of M. For the simulation parameters and pattern weight generation process described herein, a set of eight adaptive transmit patterns were generated having the magnitude and phase responses shown in Fig. 3 and Fig. 4, respectively. As illustrated in the process shown in the right-hand side of Fig. 1 these patterns are used by the clutter model to generate a new clutter covariance matrix using adaptive transmit patterns, labelled $\mathbf{R}_{ca}$.

The adapted transmit patterns exhibit some interesting characteristics. First, there are four distinct magnitude patterns as shown in Fig. 3. Close investigation shows that the magnitude patterns are symmetric about the middle of the CPI; i.e. the $m = 1$ and $m = 8$ patterns have identical magnitude responses, $m = 2$ and $m = 7$ patterns have identical magnitude responses, and so forth. Second, patterns having identical magnitude responses have dissimilar phase responses, as illustrated by Fig. 4 (for clarity, only the phase response of the main beamwidth is shown). It is also notable that the phase responses exhibit strong similarities among the first 4 pulses and the last 4 pulses.

Analysis of these patterns provides important insight that is key to generating reliable performance metrics. In addition to the modification in $\boldsymbol{\chi}_c$ shown in (18), the target space-time snapshot $\boldsymbol{\chi}_t$ requires modification as well to account for pattern diversity. The modified *target space-time snapshot* is given by

$$\boldsymbol{\chi}_t = \alpha_t \tilde{\mathbf{b}}(\theta_t, \phi_t, \bar{\omega}_t) \otimes \mathbf{a}(\vartheta_t) \tag{24}$$

where α_t is the complex target voltage, $\tilde{\mathbf{b}}(\theta_t, \phi_t, \bar{\omega}_t)$ is the tar-

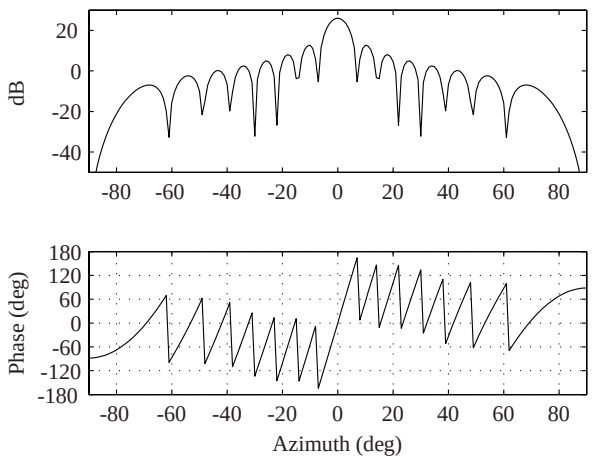

Figure 2: Transmit Pattern Magnitude (top) and Phase (bottom) Plots for Standard 16 Element Linear Array

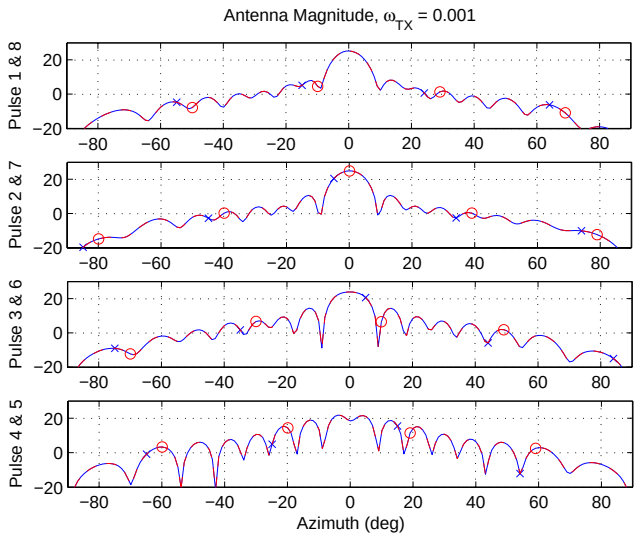

Figure 3: Magnitude of Adaptive Transmit (ATX) Patterns for 16 Element Linear Array and $M = 8$ Pulses

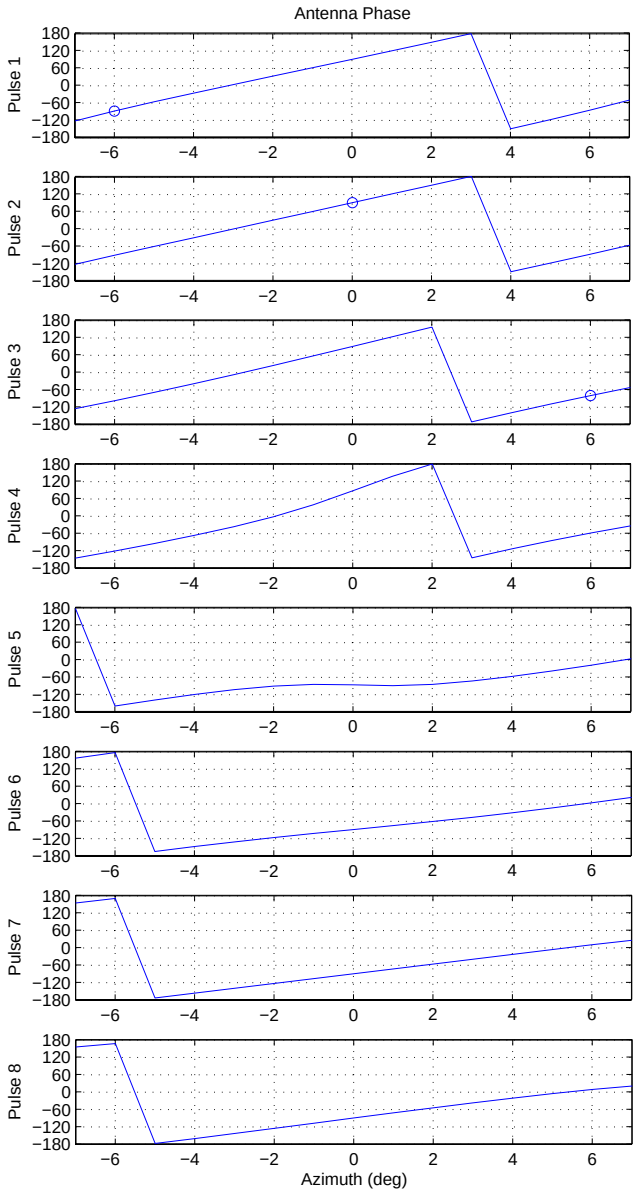

Figure 4: Phase of Adaptive Transmit (ATX) Patterns for 16 Element Linear Array and $M = 8$ Pulses

get Doppler response of (19), and $\mathbf{a}(\vartheta_t)$ is the spatial target response. Using the modified $\boldsymbol{\chi}_t$ of (24), the Output SINR metric for the case when transmit pattern diversity is employed is given by

$$\text{Output SINR} = \frac{\mathcal{E}\left\{|\mathbf{w}^H \boldsymbol{\chi}_t|^2\right\}}{\mathcal{E}\left\{|\mathbf{w}^H (\boldsymbol{\chi}_c + \boldsymbol{\chi}_n)|^2\right\}} \tag{25}$$

where $\boldsymbol{\chi}_n$ is the *thermal noise space-time snapshot*. Note that unlike a conventional target response, the elements in $\boldsymbol{\chi}_t$ of (24) and (25) fluctuate in magnitude. Although the radiated power per pulse is held constant, the adapted transmit patterns do not necessarily exhibit constant mainbeam gain toward the target on every pulse, as can be seen by the patterns in Fig. 3. In comparing output SINR results for STX and ATX scenarios, the analysis must take into account the interpulse target power variations due to ATX processing. With non-adaptive transmit patterns this was not an issue, however, with ATX it becomes an important consideration. For example, in viewing the ATX transmit weights as space-time filter weights, it is important to note that normalizing the transmit weights to achieve fixed energy per pulse corrupts the integrity of the optimum STAP weight vector (used as transmit weights) by scaling M sized sets of N weights independently. To maintain the proper scaling of the optimal STAP weights across M pulses, all transmit weights must be scaled the same. The impact of the transmit weight scaling will be demonstrated in the next section.

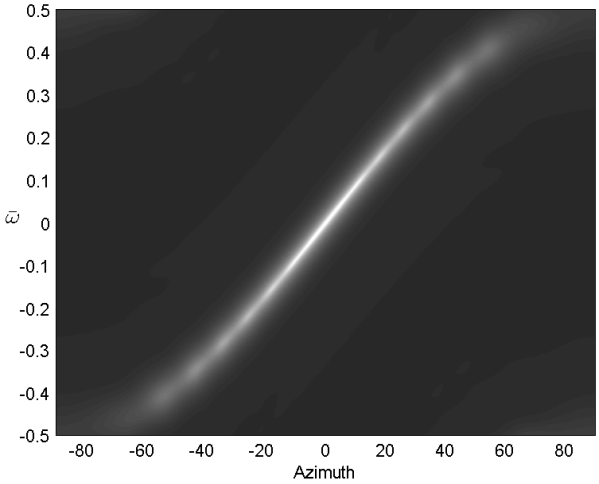

Figure 5: Azimuth-Doppler Clutter Power Spectrum of R

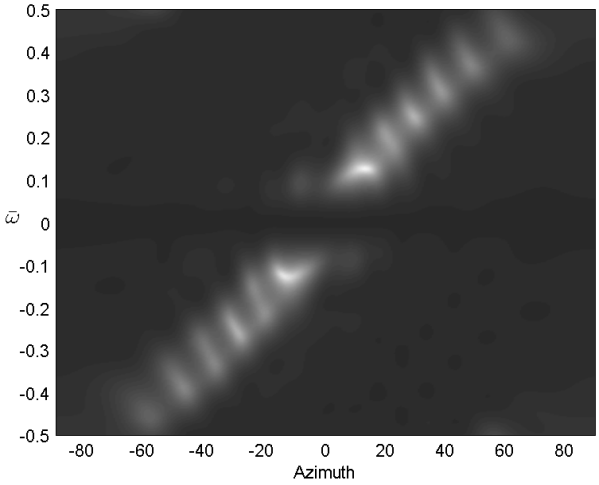

Figure 6: Azimuth-Doppler Clutter Power Spectrum of R_a

4. *SIMULATION RESULTS*

It is insightful to examine how adaptive transmit techniques change the the azimuth-Doppler clutter power spectrum. Figure 5 shows the minimum-variance clutter power spectral density of $\mathbf{R}$ in Fig. 1 for an $N = 16$ element, $M = 8$ pulse system transmitting boresight from a side-looking array. Figure 6 shows how the clutter spectrum of $\mathbf{R_a}$ from Fig. 1 changes when adaptive transmit patterns are employed. Clearly, the clutter power is being "mapped" to other locations in azimuth and Doppler by the adaptive transmit patterns. This result is not too surprising given that the main clutter model modification involves multiplication of complex weight vector $\mathbf{W}(\theta_i, \phi_k)$ with

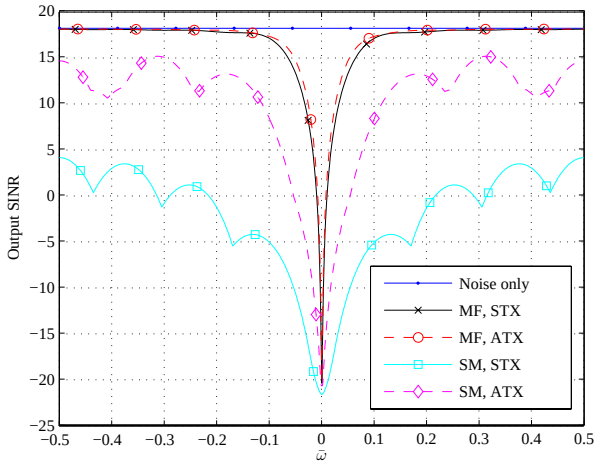

Figure 7: Output SINR results using Standard Transmit (STX) and Adaptive Transmit (ATX) techniques with $\bar{\omega}_{\mathrm{TX}} = \bar{\omega}_{\mathrm{Tgt}}$.

the Doppler steering vector $\mathbf{b}(\bar{\omega}_{ik})$ as shown in (19).

The corresponding output SINR results for standard (STX) and adaptive (ATX) transmit are provided in Fig. 7. When generating ATX results, the transmit Doppler was matched to the target Doppler for every normalized Doppler value shown. The ATX technique is shown to slightly improve minimum discernable velocity (MDV) over the MF near the main-beam clutter, an improvement made possible because transmit IPD changes the clutter power spectrum before it is received. These results were attained by normalizing the ATX weights across the CPI. When the ATX weights are normalized such that there is fixed energy per pulse, ATX performance matches that of the Matched Filter (MF) under STX. It is also clear that the non-adaptive Signal Match (SM) processor using ATX (SM-ATX) achieves much better performance that the same processor under the standard transmit model (SM-STX). This is attributed to clutter energy being spread across azimuth and doppler which provides a whitening effect on the interference.

5. CONCLUSION

This paper provides a first-look at using interpulse (pulse-to-pulse) transmit pattern diversity across the Coherent Processing Interval (CPI) of data processed via Space-Time Adaptive Processing (STAP). The speed and flexibility of modern Active Electronically Scanned Array (AESA) technology gives rise to the possibility of implementing interpulse pattern diversity to achieve improved Signal to Interference-plus-Noise Ratio (SINR). The slight narrowing of the clutter null using ATX demonstrates some promise for achieving better Minimum Discernable Velocity (MDV) using *transmit* phased array weights derived from optimum (known covariance) STAP weights. This work shows that interpulse pattern diversity using STAP-derived weights effectively re-distributes clutter energy away from the clutter ridge region. By extending this technique to planar arrays, it is hoped that this pre-whitening effect may prove effective at improving clutter covariance estimation and possibly regularizing training data for improving STAP performance in spiky, heterogeneous clutter environments.

REFERENCES

[1] J. R. Guerci, "Kassper overview," Technical Workshop Presentation, April 2002, available at http://sunrise.deepthought.rl.af.mil/kassper_html/kassper.

[2] J. Guerci and S. Pillai, "Adaptive transmission radar: the next wave," in *National Aerospace and Electronics Conference, 2000. NAECON 2000. Proceedings of the IEEE 2000*, 2000, pp. 779–786.

[3] D. Garren, M. Osborn, A. Odom, J. Goldstein, S. Pillai, and J. Guerci, "Enhanced target detection and identification via optimised radar transmission pulse shape," *Radar, Sonar and Navigation, IEE Proceedings* -, vol. 148, no. 3, pp. 130–138, 2001.

[4] D. Garren, A. Odom, M. Osborn, J. Goldstein, S. Pillai, and J. Guerci, "Full-polarization matched-illumination for target detection and identification," *Aerospace and Electronic Systems, IEEE Transactions on*, vol. 38, no. 3, pp. 824–837, 2002.

[5] S. Sowelam and A. Tewfik, "Waveform selection in radar target classification," *Information Theory, IEEE Transactions on*, vol. 46, no. 3, pp. 1014–1029, 2000.

[6] S. Pillai, J. Guerci, and S. Pillai, "Joint optimal Tx-Rx design for multiple target identification problem," in *Sensor Array and Multichannel Signal Processing Workshop Proceedings, 2002*, 2002, pp. 553–556.

[7] S. Pillai, H. Oh, D. Youla, and J. Guerci, "Optimal transmit-receiver design in the presence of signal-dependent interference and channel noise," *Information Theory, IEEE Transactions on*, vol. 46, no. 2, pp. 577–584, 2000.

[8] G. W. Stimson, *Introduction to Airborne Radar*, 2nd ed. Mendham, NJ: SciTech Publishing, Inc., 1998.

[9] A. Jaffer, M. Baker, W. Ballance, and J. Staub, "Adaptive space-time processing techniques for airborne radars," Hughes Aircraft Company, Fullerton, CA 92634, Contract F30602-89-D-0028, July 1991.

[10] J. Ward, "Space-time adaptive processing for airborne radar," Lincoln Laboratory, Massachusetts Institute of Technology, Lexington, Massachusetts, Contract F19628-95-C-0002, December 1994.

[11] R. Klemm, *Principles of Space-Time Adaptive Processing*, ser. IEE Radar, Sonar, Navigation and Avionics Series, E. D. R. Shearman and N. Stewart, Eds. Michael Faraday House, Six Hills Way, Stevenage, Herts. SG1 2AY, United Kingdom: The Institution of Electrical Engineers, 2002, vol. 12, iSBN 0852961723.

[12] C. Balanis, *Antenna Theory*, 2nd ed. New York, NY: John Wiley & Sons, Inc., 1997.

"The views expressed in this article are those of the author(s) and do not reflect official policy of the United States Air Force, Department of Defense or the U.S. Government."